scientific reports

Check for updates

OPEN

Biophysical and aerodynamic properties of a peptide targeting the A-kinase anchoring function of PI3Kγ for pulmonary cAMP modulation

Angela Della Sala[1,8], Valentina Sala[1,2,8], Cosmin Stefan Butnarasu[1], Laura Tasca[1,2], Gabriella Costabile[3], Marco Mergiotti[1], Andrea Gramegna[4,5], Francesco Blasi[4,5], Stefano Aliberti[6,7], Francesca Ungaro[3], Sonja Visentin[1], Emilio Hirsch[1,2] & Alessandra Ghigo[1,2]✉

Cyclic AMP (cAMP) signaling specificity relies on precise spatial regulation mediated by A-kinase anchoring proteins (AKAPs), which localize protein kinase A (PKA) within defined microdomains. Dysregulated AKAP signaling contributes to different pathologies, including chronic inflammatory airway diseases, making AKAP disruptors attractive therapeutic candidates. We previously showed that a cell-permeable PI3Kγ mimetic peptide (PI3Kγ MP, also known as KIT2014) that disrupts the interaction between the AKAP PI3Kγ and PKA enhances β_2-adrenergic receptordriven cAMP signaling to promote airway relaxation, mucus clearance, and reduced inflammation. Here, we investigated the structural, biophysical, and aerodynamic properties of PI3Kγ MP to gain deeper mechanistic insight. The peptide adopted a partially structured conformation essential for PKA binding, assembled into dynamic nanoparticles compatible with epithelial and mucus penetration, and retained biological activity in protease-rich environments, such as cystic fibrosis sputum. Aerodynamic profiling further demonstrated mass median aerodynamic diameters suitable for deep lung deposition upon nebulization. Collectively, these results position PI3Kγ MP as a first-in-class disruptor of the PI3Kγ-PKA complex with strong translational potential as an inhaled therapy for obstructive airway diseases driven by cAMP dysregulation.

Keywords PI3Kγ, Mimetic peptide, cAMP, AKAP, Inhaled therapy, Obstructive airway diseases

A-kinase anchoring proteins (AKAPs) orchestrate cyclic AMP (cAMP) signaling by tethering protein kinase A (PKA) and associated effectors to specific subcellular compartments. This spatial organization ensures cAMP signaling specificity and enables precise regulation of diverse physiological processes, including cardiac contractility, insulin secretion, and neuronal function. Dysregulation of AKAP-mediated signaling has been implicated in cardiovascular, neuronal and metabolic disorders, as well as cancer[1]. Consequently, peptides and peptidomimetics that selectively disrupt AKAP-based signaling complexes have emerged as powerful tools for probing compartmentalized cAMP signaling and as promising therapeutic candidates[2].

Our previous work identified phosphoinositide 3-kinase γ (PI3Kγ) as a non-canonical AKAP that regulates cAMP compartmentalization in the lung[3]. Cell-permeable mimetic peptides targeting the PI3Kγ-PKA interaction

[1]Department of Molecular Biotechnology and Health Sciences, Molecular Biotechnology Center "Guido Tarone", University of Torino, Via Nizza 52, Turin 10126, Italy. [2]Kither Biotech Srl, Turin 10126, Italy. [3]Department of Pharmacy, Federico II University, Naples, Italy. [4]Internal Medicine Department, Respiratory Unit and Cystic Fibrosis Center, Fondazione IRCCS Ca' Granda Ospedale Maggiore Policlinico, Milan 20122, Italy. [5]Department of Pathophysiology and Transplantation, University of Milan, Milan 20122, Italy. [6]Department of Biomedical Sciences, Humanitas University, Via Rita Levi Montalcini 4, Pieve Emanuele, Milan 20072, Italy. [7]IRCCS Humanitas Research Hospital, Respiratory Unit, Via Manzoni 56, Rozzano, Milan 20089, Italy. [8]Angela Della Sala and Valentina Sala contributed equally to this work. ✉email: alessandra.ghigo@unito.it

uncouple PKA from PI3Kγ-associated phosphodiesterases (PDEs), preventing their activation and thereby limiting local cAMP degradation downstream of β_2-adrenergic receptors[3,4]. This targeted modulation of cAMP signaling enhances airway smooth muscle relaxation, reduces neutrophilic inflammation, and promotes ion transport and mucus clearance[3,4]. These effects are particularly relevant for obstructive airway diseases such as asthma, chronic obstructive pulmonary disease (COPD), and cystic fibrosis (CF), all of which are characterized by airway hyperresponsiveness, chronic inflammation, and excessive mucus production[5]. Consistent with this mechanism, inhaled delivery of a PI3Kγ mimetic peptide (PI3Kγ MP, also known as KIT2014) in a murine model of chronic airway inflammation induces bronchodilation while reducing inflammation and mucus accumulation[3].

Inhalation is the preferred route for treating obstructive airway diseases, providing targeted drug delivery to the lungs, minimizing systemic exposure, and ensuring a rapid onset of action[6,7]. However, the pathological alterations in diseased lungs create substantial barriers to effective drug delivery. In CF, for example, highly viscous and adhesive mucus, impaired mucociliary clearance, persistent inflammation, and protease-rich environments can impede drug diffusion, accelerate degradation, and limit cellular uptake. Beyond overcoming these biochemical and structural barriers, inhaled formulations must also exhibit aerodynamic properties that ensure deep-lung deposition while minimizing oropharyngeal deposition and swallowing[6].

Here, we investigated the structural, biophysical, and aerodynamic properties of PI3Kγ MP to clarify its mechanism of action as an inhaled therapy for lung disease. We demonstrate that the peptide adopted a partially structured conformation critical for target binding, assembled into nanoparticles compatible with permeability across cellular membranes and pathological mucus, and retained biological activity in protease-rich environments. In addition, PI3Kγ MP displayed aerodynamic properties suitable for efficient deep-lung deposition. Overall, these findings support the feasibility of inhaled PI3Kγ MP as a targeted therapeutic strategy for obstructive airway diseases.

Results

PI3Kγ MP adopts a partially structured conformation

To gain deeper mechanistic insight into PI3Kγ MP, we first analyzed its predicted three-dimensional conformation. PI3Kγ MP comprises the cell-penetrating peptide Penetratin-1 (P1), a glycine linker, and the PKA-binding motif of PI3Kγ spanning residues 126–150 (Fig. 1a). In silico modeling predicted an α-helical segment primarily within P1, flanked by an unstructured region corresponding to the PI3Kγ-derived sequence (Fig. 1b). This prediction was supported by circular dichroism (CD) spectroscopy, which exhibited a characteristic double signal: a maximum near 200 nm, indicative of random coil elements, and a weak negative band around 220–240 nm, consistent with limited α-helical content[8] (Fig. 1c). Spectral deconvolution confirmed a largely disordered conformation with minor but notable secondary structure elements (~ 8% α-helix, 22% β-strand; Fig. 1c). In silico docking simulations of PI3Kγ MP with the PKA regulatory subunit PKA-RIIα, the native binding partner of PI3Kγ[4], revealed a preferential binding interface involving hydrophilic residues within K18-Q40 of PI3Kγ MP (Fig. 1d-e). In contrast, PKA-RIIα showed no detectable interaction with the cell-penetrating segment P1 (Fig. 1d, e), indicating that binding specificity resides in the PI3Kγ-derived sequence. Collectively, these findings demonstrate that PI3Kγ MP adopts a partially structured conformation and selectively interacts with PKA-RIIα through its PI3Kγ-derived domain.

PI3Kγ MP overcomes cellular and biological barriers

Next, we investigated the molecular dimensions of the peptide and its capacity to traverse cellular barriers. Transmission electron microscopy (TEM) revealed that PI3Kγ MP formed irregular nanoparticles up to 500 nm in size (Fig. 2a). This aggregation tendency was corroborated by dynamic light scattering (DLS), which indicated particle sizes of 200–300 nm (Fig. 2b). Notably, treatment with hexafluoroisopropanol (HFIP), a solvent known to induce protein cold denaturation, reduced aggregate size to ~ 10 nm (Fig. 2b), demonstrating that aggregation is reversible and solvent-sensitive.

We next evaluated the membrane permeability of the peptide. In vitro lipophilicity assessment revealed a low partition coefficient ($logD_{7.4} = 0.25$), indicating that the peptide predominantly partitions into the aqueous phase (Table 1) and suggesting limited potential for passive transmembrane diffusion. Transport studies in MDCKII cell monolayers, a gold-standard epithelial model for ADME and permeability studies of inhaled biologics[9,10], showed significant peptide clearance from donor compartments (62% A-B direction, 36% B-A direction) with minimal appearance in receiver chambers (Table 2), which indicates efficient cellular uptake and intracellular retention. These findings demonstrate that the peptide achieves substantial cellular internalization, likely through the P1 module-mediated active transport mechanism.

To evaluate the permeability of PI3Kγ MP under disease-relevant conditions, we performed a Parallel Artificial Membrane Permeability Assay (PAMPA) incorporating a mucus layer that mimics pathological lung secretions. When CF sputum, used as a surrogate for the airway mucus in CF patients, was applied to the phospholipid membrane (Fig. 2c), the apparent permeability (P_{app}) decreased to 1.46×10^{-6} cm s^{-1} (Fig. 2d) yet remained within the range typical of compounds with moderate to high permeability[11].

These results demonstrate that PI3Kγ MP can cross both cellular barriers and pathological mucus layers, underscoring its potential for therapeutic delivery in obstructive airway diseases.

PI3Kγ MP remains biologically active in protease-rich environments

We next assessed the proteolytic stability of PI3Kγ MP using its ability to elevate intracellular cAMP levels in human bronchial epithelial cells (16HBE14o-) as an indirect readout of functional integrity over time. PI3Kγ MP induced a sustained increase in intracellular cAMP for up to 2 h upon stimulation (Fig. 3a), indicating a good resistance to intracellular proteolytic degradation. To investigate susceptibility to extracellular proteases,

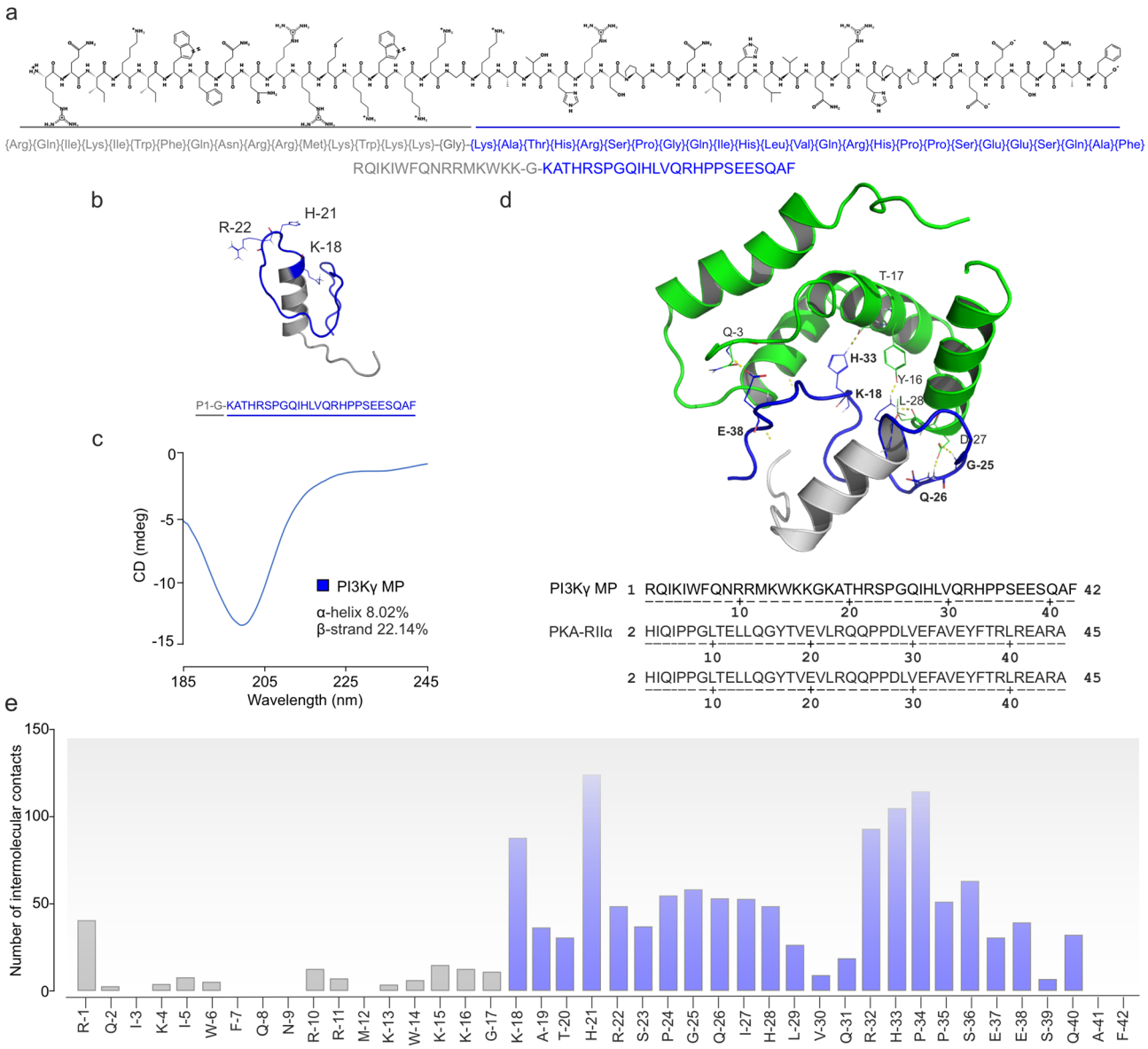

Fig. 1. Prediction of PI3Kγ MP structure and its binding to PKA-RIIα. **a**) Chemical structure of PI3Kγ MP. The amino acid sequence of PI3Kγ MP comprises the cell penetrating peptide Penetratin 1 (P1), a glycine (G) linker and the PKA-binding motif of PI3Kγ (residues 126–150: KATHRSPGQIHLVQRHPPSEESQAF). **(b)** PI3Kγ MP structure prediction by PEP-FOLD3.5. P1-G and residues 126–150 of PI3Kγ are shown as cartoons in grey and blue, respectively. R-22, H-21 and K-18 residues are indicated and shown as sticks. **(c)** Circular dichroism spectra of PI3Kγ MP showing a peak at 190–220 nm. The percentage of α-helical and β-sheet secondary structures calculated by the K2D2 web server are indicated. **(d)** Molecular docking simulation of the interaction between PI3Kγ MP and the PKA-RIIα dimer by HADDOCK 2.4. The docked pose of PI3Kγ MP in complex with residues 2 to 44 of the PKA-RIIα dimer (cartoon in green) is shown. The key residues involved in the binding are indicated and shown as sticks, with PI3Kγ MP residues in bold. Hydrogen bonds between PI3Kγ MP and PKA-RIIα are indicated by yellow dashed lines. **(e)** Number of intermolecular contacts between PI3Kγ MP with partners in the PKA-RIIα dimer (2–44 PKA-RIIα) by PROtein binDIng enerGY prediction (PRODIGY). The number of intermolecular contacts involving P1-G and residues 18–42 of PI3Kγ MP (corresponding to amino acids 126–150 of PI3Kγ) are represented as grey and blue bars, respectively. In **b** and **d**, the structural models were developed using PyMOL.

we focused on neutrophil elastase, a major protease commonly found in diseased lungs, such as those affected by CF and bronchiectasis[12]. In silico analysis identified three potential cleavage sites for human neutrophil elastase (HNE) within the PI3Kγ MP sequence (Fig. 3b), indicating a possible susceptibility to proteolytic degradation. However, despite these predictions, PI3Kγ MP retained up to 62% of its cAMP-inducing activity after exposure to 3 µg/mL recombinant HNE (Fig. 3c), a concentration previously shown to inactivate other therapeutic peptides[13]. Notably, this stability was preserved even at a tenfold higher HNE concentration (30 µg/mL) (Fig.

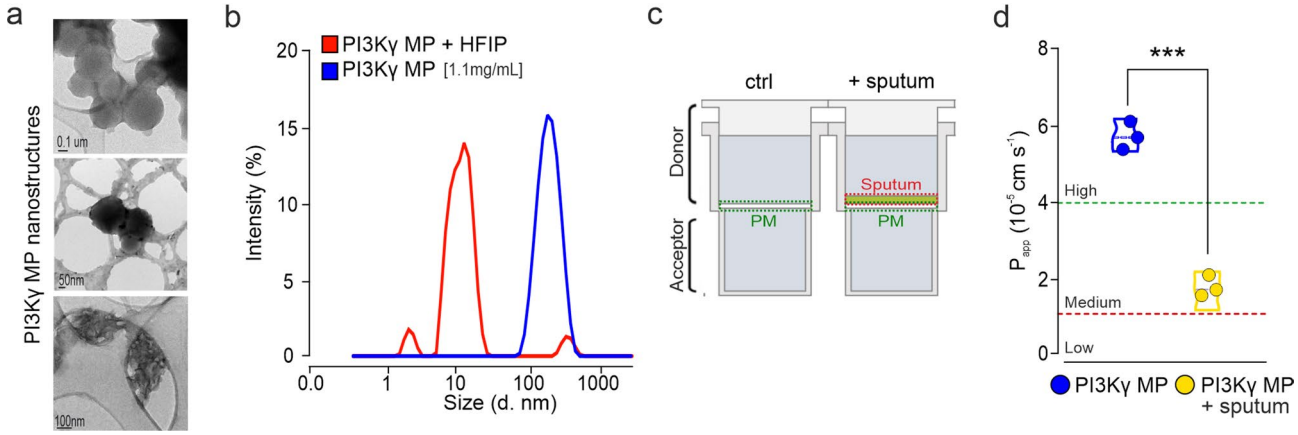

Fig. 2. PI3Kγ MP can penetrate pathological mucus. **a)** Representative transmission electron microscopy (TEM) images of PI3Kγ MP (0.1 mg/mL in water). **b)** Size distribution profile of PI3Kγ MP (1.1 mg/mL in 2 mM PBS) obtained by dynamic light scattering (DLS) analysis in the absence (blue trace) and in the presence of hexafluoroisopropanol (HFIP, red trace). **c)** Schematic representation of the Parallel Artificial Membrane Permeability Assay (PAMPA) with and without deposition of cystic fibrosis (CF) sputum on top of the artificial lipid membrane (PM). **d**) Apparent permeability (P_{app}) measurements of PI3Kγ MP (2 mg/mL), in the absence (blue box) and in the presence (yellow box) of CF sputum. The green dashed line indicates the threshold P_{app} for high-medium permeable compounds (4×10^{-6} cm s^{-1}), while the red dashed line defines the limit for medium-low permeable molecules (1×10^{-6} cm s^{-1})[11].

Compound	logD
PI3Kγ MP	0.25
Simvastatin	> 4.32
Tamoxifen	> 5.38
Haloperidol	2.59
Ketoconazole	3.42
Metoprolol tartrate	-0.57
Phenytoin	2.36
Rifampicin	1.02

Table 1. In vitro partitioning of PI3Kγ MP. Simvastatin, Tamoxifen, Haloperidol, Ketoconazole, Metoprolol tartrate, Phenytoin and Rifampicin were used as reference compounds. Test compounds concentration 1.0 $*10^{-5}$ M. LogD: Partition coefficient.

	Permeability A-B	Recovery (%) A-B	Permeability B-A	Recovery (%) B-A
PI3Kγ MP	< 0.356 ± 0.01	38	< 0.135 ± 0.007	64
Colchicine	1.2 ± 0.21	85	2.5 ± 0.31	81
Propranolol	41.8 ± 1.11	70	21.3 ± 1.29	90
Ranitidine	1.5 ± 0.11	91	2.1 ± 0.007	93

Table 2. In vitro absorption of PI3Kγ MP in MDCKII cells. Colchicine, Propranolol and Ranitidine were used as reference compounds of transporter-mediated, high, and low permeability, respectively. Test compounds concentration 1.0 $*10^{-5}$ M. $N = 2$ independent experiments. Permeability units are expressed as 10^{-6} cm/s. Throughout, data are means ± standard deviation.

3d), reflecting protease levels typically found in the lungs of patients with severe bronchiectasis[12]. Moreover, when tested in the presence of CF sputum, a complex and protease-rich biological matrix, PI3Kγ MP maintained up to 52% of its biological activity (Fig. 3e), further supporting its proteolytic resilience under physiologically relevant conditions.

Collectively, these results demonstrate that PI3Kγ MP retains significant biological activity in protease-rich environments, highlighting its relative resistance to degradation and its suitability for therapeutic application in inflamed, mucus-obstructed airways.

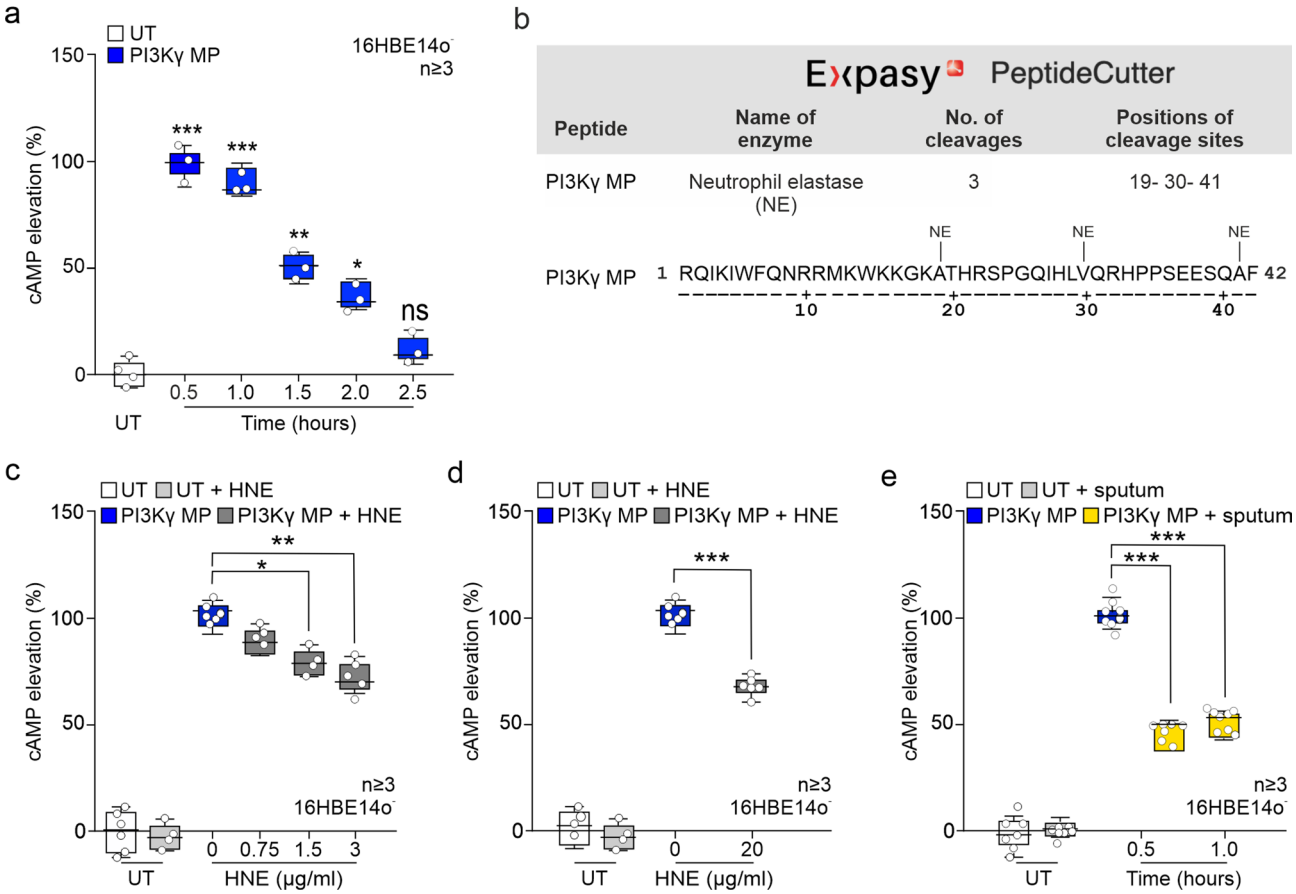

Fig. 3. PI3Kγ MP is resistant to protease degradation. **(a)** cAMP elevation in 16HBE14o- cells at the indicated time points after treatment with 25 μM PI3Kγ MP. The amount of cAMP was expressed as percentage of cAMP accumulation elicited by PI3Kγ MP at 30 min. $n \geq 3$ technical replicates from $N = 3$ independent experiments. $^{***}P < 0.001$ *versus* untreated (UT) by one-way ANOVA, followed by Bonferroni's post hoc test. (**b**) Prediction of neutrophil elastase (NE) cleavage sites within the PI3Kγ MP sequence via Expasy PeptideCutter software. **c**-**d**) cAMP concentration in 16HBE14o- cells treated with the PI3Kγ MP (25 μM for 30 min) in the absence (blue box) and in the presence (gray boxes) of either a low dose (0.75-1.5-3 μg/mL; **c**) or a high dose (20 μg/mL; **d**) of human neutrophil elastase (HNE). The amount of cAMP was expressed as percentage of cAMP accumulation elicited by PI3Kγ MP without HNE. $n \geq 3$ technical replicates from $N > 3$ independent experiments. $^{*}P < 0.05$, $^{**}P < 0.01$ and $^{***}P < 0.001$ by one-way ANOVA, followed by Bonferroni's post hoc test. **e)** cAMP elevation in 16HBE14o- cells covered with a layer of CF sputum and then treated with 25 μM PI3Kγ MP for 30 min and 1 h. The amount of cAMP was expressed as percentage of cAMP accumulation elicited by PI3Kγ MP in the absence of sputum at 30 min. $^{***}P < 0.001$ *versus* PI3Kγ MP without sputum by two-way ANOVA test, followed by Bonferroni's post-hoc analysis. $n \geq 6$ technical replicates from $N = 3$ independent experiments. Throughout, data are means ± SEM.

PI3Kγ MP can be effectively delivered to the lower respiratory airways

To confirm the suitability of PI3Kγ MP for pulmonary delivery via aerosolization, we evaluated its aerodynamic properties. The peptide was nebulized using three devices commonly employed for CF therapy[14]: a jet nebulizer (TurboBoy) and two vibrating mesh nebulizers (Aeroneb® Go and PARI eFlow® Rapid). The aerosol was drawn through the Next Generation Impactor (NGI), which separates particles across seven stages based on aerodynamic diameter (Fig. 4a). Figure 4b describes the cumulative droplet size distribution of the emitted dose. In each case, the best fit line was from logarithmic linear regression (r2 ≥ 0.94). Across all devices, the mass median aerodynamic diameter (MMAD) ranged from 2.0 to 2.99 μm (Table 3), an optimal range for deep lung deposition as particles smaller than 5 μm can typically reach the bronchi and alveoli[15]. Despite similar MMAD values, deposition profiles differed slightly among the devices (Fig. 4c). Regardless of the device, minimal deposition occurred in the NGI stages representing the oropharyngeal region (i.e., throat and S1), suggesting a low risk of peptide loss via swallowing or off-target gastrointestinal exposure. Nonetheless, the vibrating mesh nebulizers significantly outperformed the jet nebulizer, delivering emitted doses exceeding 40%, nearly twice the amount achieved by the TurboBoy device (Fig. 4d; Table 3). This superiority was further supported by the respirable fraction (RF), that is the proportion of peptide recovered from NGI stages likely to reach the lungs, which surpassed 90% for both mesh nebulizers (Table 3), indicating highly efficient delivery to the lower respiratory tract. Finally, to verify that aerosolization did not compromise the biological activity of the peptide, PI3Kγ

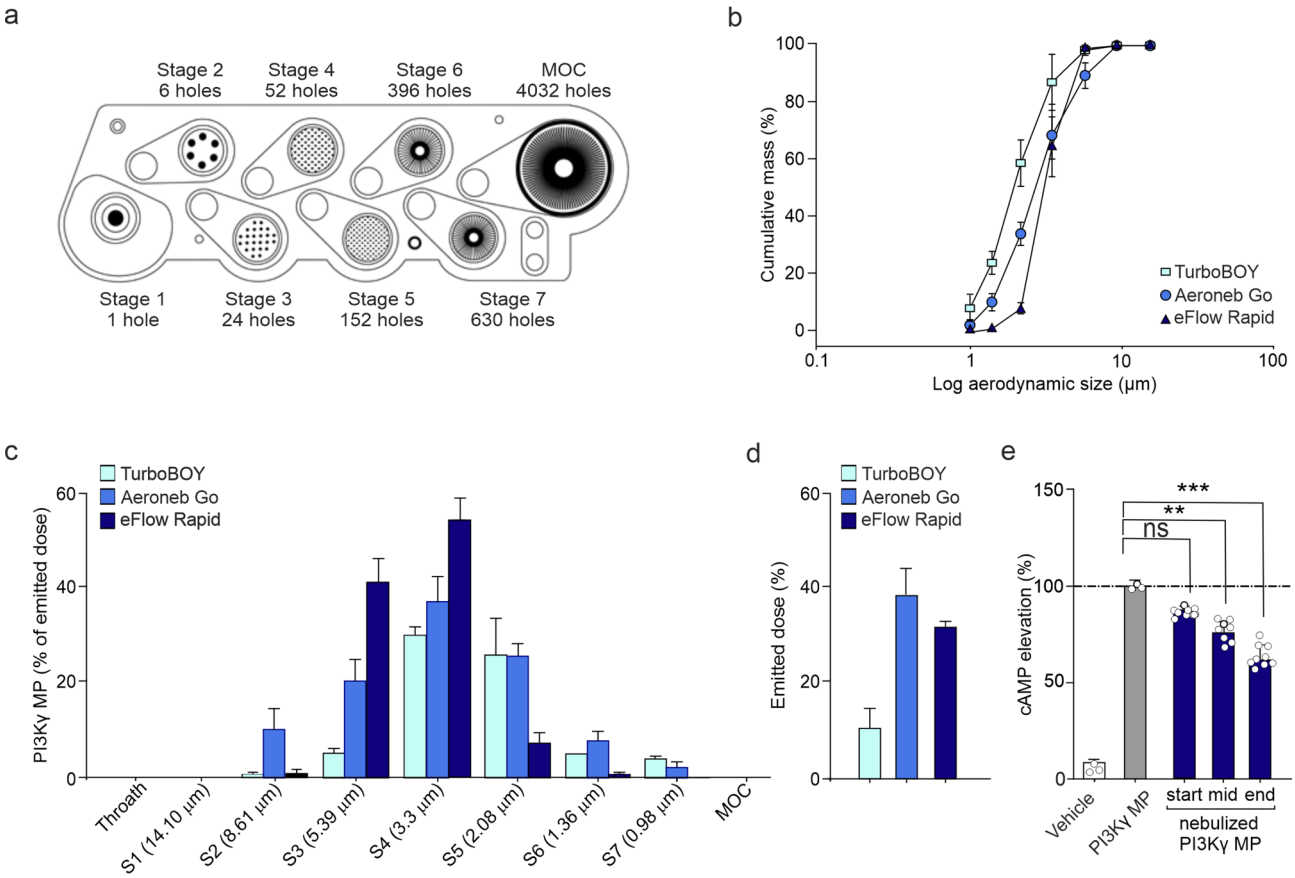

Fig. 4. Aerodynamic properties of PI3Kγ MP. **(a)** Schematic representation of the Next Generation Impactor (NGI) apparatus equipped with seven stages cups (S1-S7) and a micro-orifice collector (MOC). **(b)** Cumulative droplet size distribution of the emitted dose of PI3Kγ MP after nebulization with three devices (one jet nebulizer –TurboBoy- and two mesh nebulizers – Aeroneb® Go and PARI eFlow® Rapid). **c-d)** In vitro aerosol performance of PI3Kγ MP after nebulization with the three devices. In **c)**, cumulative mass of PI3Kγ MP recovered in the different stages expressed as a function of the cut-off diameter of the NGI and of the emitted dose. In **d)**, the emitted dose of PI3Kγ MP, representing the total mass of peptide emitted from the NGI. Data are means ± SD. **e)** cAMP elevation in 16HBE14o- cells treated with the peptide recovered at the beginning, middle, and end of the nebulization process with eFlow rapid. The amount of cAMP was expressed as percentage of cAMP accumulation elicited by non-nebulized PI3Kγ MP. $^{**}P < 0.01$ and $^{***}P < 0.001$ *versus* non-nebulized PI3Kγ MP by two-way ANOVA test, followed by Bonferroni's post-hoc analysis. $n \geq 3$ technical replicates from $N = 3$ independent experiments. Data are means ± SEM.

MP was nebulized using the PARI eFlow® Rapid device and collected at the beginning, middle, and end of the process. All samples retained the ability to elevate intracellular cAMP levels in 16HBE14o- cells, comparable to the non-nebulized control (Fig. 4e), confirming that functional integrity was preserved throughout nebulization.

Altogether, these results demonstrate that PI3Kγ MP exhibits favorable aerodynamic and physicochemical properties for inhaled delivery. Its efficient lung targeting, high respirable fraction, and preserved biological activity following nebulization support its potential as a viable therapeutic candidate for modulating cAMP signaling in the diseased airways.

Discussion

The present characterization of the biophysical and aerodynamic properties of PI3Kγ MP provides new insight into how PI3Kγ mimetic peptides engage their molecular target and exert therapeutic effects in chronic obstructive airway diseases, including CF[3,4]. The pharmacological activity of PI3Kγ MP depends on its ability to displace PKA from the PI3Kγ complex, without altering the kinase-dependent catalytic activity of PI3Kγ or downstream Akt signaling[3]. By selectively targeting the scaffold function of PI3Kγ, the peptide prevents PKA-mediated activation of a PDE4 pool that regulates β_2-adrenergic receptor/cAMP signaling in bronchial smooth muscle, immune, and epithelial cells[3]. Our findings now demonstrate that this displacement is mediated by the peptide adopting a partially structured conformation. The PI3Kγ-derived segment (residues 126–150) remains largely disordered yet forms multiple intermolecular contacts with PKA-RII, enabling effective competition with native PI3Kγ for binding[4]. In silico modeling further indicates that most secondary structure elements, particularly the α-helix, map to the cell-penetrating motif P1. This observation is consistent with the

	TurboBoy	AeronebGo	eFlow rapid
$MMAD_{exp}$ (µm ± SD)	2.00 ± 0.091	2.70 ± 0.305	2.99 ± 0.068
GSD (± SD)	1.94 ± 0.308	2.10 ± 0.234	1.85 ± 0.013
FPF (± SD)	ND	43.2 ± 11.1	38.9 ± 1.17
RF (± SD)	ND	90.3 ± 6.08	99.0 ± 0.75

Table 3. Fine particle characteristics of the aerosol clouds generated upon delivery of a PI3Kγ MP aqueous dispersion through either jet (PARI TurboBoy) or VMT (AeronebGo® and PARI eFlow® rapid) nebulizers. $MMAD_{exp}$ = Experimental Mass Mean Aerodynamic Diameter; GSD = Geometric Standard Deviation; FPF = Fine Particle Fraction; RF = Respirable Fraction. $MMAD_{exp}$ and GSD were calculated from the logarithmic linear regression according to Ph.Eur. FPF was calculated on the nominal PI3Kγ MP dose, whereas the RF refers to the emitted dose of PI3Kγ MP. Data are reported as means ± standard deviation (SD) of triplicate experiments.

well-documented propensity of cell-penetrating peptides to adopt an amphipathic α-helical conformation, a structural feature essential for membrane perturbation and direct bilayer translocation[7]. Our results underscore the essential role of P1-mediated active transport in driving cellular uptake of PI3Kγ MP. Although distribution assays indicated high hydrophilicity, an intrinsic property that would typically restrict passive diffusion across lipid membranes, PI3Kγ MP nevertheless exhibited high permeability in both PAMPA and epithelial cell-based assays. These findings are consistent with our previous observations in human bronchial smooth muscle cells[3]. This apparent paradox can be explained by the presence of P1, which actively mediates translocation across the plasma membrane, thereby overcoming the limitations imposed by hydrophilicity. Notably, once internalized, PI3Kγ MP shows strong intracellular retention with minimal efflux, an important property for sustaining therapeutic activity.

Cell membranes represent only one of several barriers to inhaled drugs. In obstructive airway diseases, an abnormally thick mucus layer, enriched with proteolytic enzymes, poses an additional challenge[6]. Our results indicate that PI3Kγ MP can partially overcome these barriers. The permeability of the peptide was slightly reduced in the presence of CF patient-derived sputum, used here as a proxy for the pathological mucus found in CF airways. This reduction is likely due to the smaller mesh size of diseased mucus (60–300 nm) compared to physiological mucus (≈ 500 nm)[16,17], which may impede the diffusion of larger peptide nanoparticles. TEM and DLS analyses revealed that PI3Kγ MP tends to form nanoparticles ranging from 200 to 500 nm, suggesting that smaller particles can navigate through mucus pores, while larger ones may be partially restricted. Despite this modest reduction, PI3Kγ MP maintained medium-to-high permeability values, supporting its potential for effective delivery in mucus-obstructed airways[11].

The elevated protease content in pathological mucus presents an additional barrier to peptide-based therapeutics. Importantly, PI3Kγ MP retained 52–62% activity in the presence of recombinant neutrophil elastase and CF sputum, indicating partial protease resistance. This stability likely reflects rapid cell penetration and intracellular retention of the peptide, which minimize its exposure to extracellular proteases. These findings provide a mechanistic explanation for our previous observation that aerosolized PI3Kγ MP exerts therapeutically relevant effects in vivo in a murine model of inflammatory airway disease characterized by mucus hypersecretion and neutrophilic inflammation, both key sources of elastase activity[3]. In the ovalbumin-induced model of allergic airway inflammation, PI3Kγ MP administration significantly promoted airway relaxation, as demonstrated by inhibition of methacholine-induced bronchoconstriction, despite the protease- and sputum-rich environment. These in vivo results demonstrate that the residual activity of the peptide observed in vitro following elastase and sputum exposure is sufficient to achieve meaningful therapeutic effects. This resilience is particularly relevant for neutrophilic airway diseases, including CF and COPD, where neutrophil elastase levels are markedly elevated[18].

Effective deposition in the lower airways is another prerequisite for effective inhalation therapy, requiring a respirable aerodynamic diameter (1–5 µm) and optimized device performance[14,15]. Despite its tendency to form nanoparticles, PI3Kγ MP exhibited aerodynamic properties compatible with deep-lung delivery. Importantly, minimal deposition in the upper NGI stages, representing the oropharyngeal region, suggests a low risk of gastrointestinal exposure via swallowing. Notably, among the devices tested, vibrating mesh nebulizers outperformed jet nebulizers, achieving respirable fractions > 90% and up to twice the emitted dose, making them preferable for PI3Kγ MP administration. Although no single nebulizer can be considered optimal for CF patients, mesh nebulizers, such as the PARI eFlow®, have been shown to shorten treatment times relative to conventional jet nebulizers and may enhance pulmonary drug deposition as well as patient adherence to therapy[19].

In summary, PI3Kγ MP combines essential features for effective pulmonary delivery, including robust cellular uptake, efficient mucus penetration, partial resistance to proteolytic degradation, and aerodynamic characteristics favorable for deep lung deposition. These attributes support PI3Kγ MP as a valuable candidate for targeted inhalation therapy in obstructive airway diseases.

Materials and methods

Peptides and reagents

Peptides were synthesized by GenScript (Piscataway, NJ) with a purity greater than 95%. Human neutrophil elastase was obtained from Sigma-Aldrich (CAS 9004-06-2, Sigma-Aldrich, Saint Louis, MO) and reconstituted

in 50 mM sodium acetate (pH 5.5) with 200 mM NaCl. Propranolol (CAS 318-98-9), Hexafluoroisopropanol (CAS 920-66-1), Colchicine (CAS 64-86-8), Simvastatin (CAS 79902-63-9), Tamoxifen (CAS 10540-29-1), Haloperidol (CAS 52-86-8), Ketoconazole (CAS 65277-42-1), Metoprolol Tartrate (CAS 56392-17-7), Phenytoin (CAS 57-41-0), Rifampicin (CAS 13292-46-1) and Ranitidine (CAS 66357-59-3) were purchased from Sigma-Aldrich (Sigma-Aldrich, Saint Louis, MO).

Cell lines

Immortalized normal human bronchial epithelial cells (16HBE14o-) were generously provided by Dr. Gruenert (University of California San Francisco, San Francisco, CA). Cells were maintained in Minimum Essential Medium (MEM) supplemented with 10% FBS, 5 mM L-Glutamine, 100 U/mL penicillin and 100 µg/mL streptomycin (Thermo Fisher Scientific, Waltham, MA) on culture dishes pre-coated with human fibronectin (1 mg/mL; Sigma-Aldrich, Saint Louis, MO), bovine collagen I (3 mg/mL; Sigma-Aldrich, Saint Louis, MO) and bovine serum albumin (0.1%; Sigma-Aldrich, Saint Louis, MO) diluted in LHC-8 basal medium (Invitrogen, Waltham, MA). Madin Darby Canine Kidney cells (MDCKII) were purchased from Sigma-Aldrich (CB 85011435, Sigma-Aldrich, Saint Louis, MO) and grown in Dulbecco′s Modified Eagle′s Medium (DMEM) supplemented with 10% FBS, 2 mM L-Glutamine, 100 U/mL penicillin and 100 µg/mL streptomycin (Thermo Fisher Scientific, Waltham, MA). Cells up to passage 15 were used for experiments and tested negative for mycoplasma contamination prior to use. Cells were maintained at 37 °C in a humidified incubator with 5% CO_2.

cAMP measurements

cAMP content was measured in 16HBE14o- and MDCKII cells at the indicated time points after treatment with the indicated doses of peptides using the Promega cAMP-Glo™ Assay kit (Promega, Milano, IT), according to the manufacturer's protocol.

Ethical statement

Spontaneous expectorated sputum samples from CF patients in stable clinical conditions were collected at the Bronchiectasis and Cystic Fibrosis Programs of the Respiratory Department of Fondazione IRCCS Ca' Granda Ospedale Maggiore Policlinico in Milan (Italy) and processed as previously described[20]. The study protocol was approved by the Ethics Committee of Fondazione IRCCS Ca' Granda Ospedale Maggiore Policlinico (594_2016bis). All methods were performed in accordance with the relevant guidelines and regulations. All participants provided written informed consent to the collection and use of their biological samples.

CF sputum samples

Briefly, samples were first cleared of saliva, and selected sputum plugs were weighed and diluted 1:8 in phosphate-buffered saline (PBS). The mixture was vortexed until fully homogenized, then centrifuged at 3000 × g for 15 min. Supernatants were collected, aliquoted, and stored at − 80 °C. Prior to experimental use, samples were thawed overnight at 4 °C, and all assays were conducted within 24 h of thawing.

Neutrophil elastase (NE) levels were quantified as previously reported[20] and samples containing 20 µg/mL of active NE were used to assess the activity of peptides in 16HBE14o- cells. For in vitro testing, 16HBE14o- cells were seeded in 96-well plates at a density of 2×10^4 cells/well and incubated for 16/18 hours at 37 °C in a humidified 5% CO_2 atmosphere.

Subsequently, peptides were diluted in PBS to a final concentration of 25 µM, and a 1:1 mixture of PBS and CF sputum (100 µL/well) was added to the adherent cells. cAMP levels were measured at defined time points using the cAMP-Glo™ Assay kit (Promega, Milan, Italy), following the manufacturer's instructions.

Parallel Artificial Membrane Permeability Assay (PAMPA)

To assess the permeability of peptides through a CF sputum layer, a parallel artificial membrane permeability system (PAMPA) (Corning Gentest Pre-coated PAMPA, 353015, USA plates) was performed following established protocols[11]. This system models passive diffusion by measuring the transport of compounds from a donor compartment, across an artificial membrane, into an acceptor compartment. The bottom wells of the PAMPA system ("acceptor" wells) were filled with 300 µL of PBS (10 mM phosphates, 150 mM NaCl, pH 7.4), while the "donor" wells were loaded with 200 µL of the peptide solution (2 mg/mL in PBS buffer, described above), either in the absence or presence of CF sputum. For experiments with sputum, 40 µL of homogenized sputum was layered directly onto the membrane prior to addition of the peptide solution. Sputum was homogenized using a 1 mL syringe and a 20 G cannula before use. The donor and acceptor plates were assembled and incubated for 5 h at room temperature. After incubation, the plates were separated, and peptide concentrations in the acceptor wells were quantified by fluorescence spectroscopy using a Horiba Jobin Yvon Fluorolog 3 TCSPC fluorimeter (Horiba, Kyoto, Japan) equipped with a 450-W xenon lamp and a R928 photomultiplier (Hamamatsu Photonics, Hamamatsu, Japan). Excitation was performed at 280 nm and emission was recorded in the spectral region of 290–500 nm (maximum of emission at 362 nm), with excitation and emission slits of 4 and 5 nm, respectively. PBS alone, under standard and sputum-containing conditions, was used as a blank control, and peptide concentrations were calculated after blank subtraction from fluorescence intensity. Quantification was performed using a 6-points calibration curve. The apparent permeability coefficient (P_{app}) was expressed according to this relationship:

$$P_{app} = \frac{dQ/dt}{C_0 \times A}$$

derived from Fick's law for steady-state conditions[21], where dQ is the quantity of drug expressed as moles permeated into the acceptor compartment at time t (18000 s), C_0 is the initial concentration of the peptide in the donor well, and A is the area of the well membrane (0.3 CM^2).

In vitro permeability assay in MDCKII cells

To investigate the membrane permeability properties of the peptide through cell monolayers, MDCKII (Madin–Darby canine kidney) were used as described previously[9]. MDCKII cells represent a well-established and widely validated epithelial model for ADME and permeability studies of inhaled biologics as they form well-polarized monolayers with stable tight junctions and a low endogenous transporter background[9,10]. Briefly, MDCKII cell monolayers were grown on 0.4 µm Transwell-COL membrane culture inserts and seeded at high density. MDCKII monolayers were cultured for 3 days before use. Test compounds were tested using 100 µM donor solutions in transport medium (pH 7.4) containing 1% DMSO. Fluorescein was used as an internal control to verify tight junction integrity of the cell monolayer after the permeability assay for the test compound. Monolayers with a fluorescein permeability below 2.5×10^{-6} cm/s were considered intact, and only results obtained under these conditions were reported. To benchmark the assay, propranolol, colchicine, and ranitidine were included as reference permeability compounds, representing high passive permeability, transporter-mediated permeability (P-glycoprotein substrate), and low permeability, respectively. The apparent permeability coefficient (P_{app}) of the test compounds was calculated according to the following equation:

$$P_{app}\left(\frac{cm}{s}\right) = \frac{V_R * C_{R,end}}{\Delta t} * \frac{1}{A * (C_{D,mid} - C_{R,mid})}$$

where V_R is the volume of the receiver chamber. $C_{R,\,end}$ is the concentration of the test compound in the receiver chamber at the end time point, Δt is the incubation time and A is the surface area of the cell monolayer. $C_{D,\,mid}$ is the calculated mid-point concentration of the test compound in the donor side, which is the mean value of the donor concentration at time 0 min and the donor concentration at the end time point. $C_{R,\,mid}$ is the mid-point concentration of the test compound in the receiver side, which is one half of the receiver concentration at the end time point. Concentrations of the test compound were expressed as peak areas of the test compound. The recovery of the test compound from the Permeability assay was calculated as follows:

$$\text{Recovery}\ \ (\%) = \frac{V_D * C_{D,end} + V_R * C_{R,end}}{V_D * C_{D0}} * 100$$

where V_D and V_R are the volumes of the donor and receiver chambers, respectively. $C_{D,\,end}$ is the concentration of the test compound in the donor sample at the end time point. $C_{R,\,end}$ is the concentration of the test compound in the receiver sample at the end time point. C_{D0} is the concentration of the test compound in the donor sample at time zero. Concentrations of the test compound are expressed as peak areas of the test compound. This assay was performed by Eurofins Panlabs (St. Charles, MO, USA).

In vitro partition coefficient calculation

To investigate the partitioning of the peptide in solvents, the Partition Coefficient (logD, n-octanol/PBS, pH 7.4) was measured as described previously[22]. Briefly, the test compound, at a concentration of 100 µM, was incubated in a shaking flask at room temperature for 60 min and then analyzed by HPLC-UV/VIS. The total amount of compound was determined as the peak area of the principal peak in a calibration standard (100 µM) containing organic solvent (methanol/water, 60/40, v/v). The amount of compound in buffer was determined as the combined, volume-corrected, and weighted areas of the corresponding peaks in the aqueous phases (PBS, pH 7.4) of three organic-aqueous samples of different composition. An automated weighting system was used to ensure the preferred use of raw data from those samples with well quantifiable peak signals. The amount of compound in organic (n-octanol) was calculated by subtraction. Subsequently, logD was calculated as the $\log_{10}$ of the amount of compound in the organic phase divided by the amount of compound in the aqueous phase. This assay was performed by Eurofins Panlabs (St. Charles, MO, USA).

Next Generation Impactor (NGI) studies

The aerodynamic properties of the peptide were assessed using a Next Generation Impactor (NGI) (Copley Scientific, Nottingham, UK), according to the Comité Européen de Normalization standard methodology for nebulizer systems. The NGI equipment consisted of seven stages cups (S1-S7), a micro-orifice collector (MOC), an induction port and a vacuum pump simulating inspiration. Three nebulizer devices were tested: one jet nebulizer – TurboBoy (PARI TurboBOY, PARI GmbH, Starnberg, Germany), and two mesh nebulizers – AeronebGo (Aeroneb® Go, Aerogen Ltd., Galway, Ireland) and – eFlow rapid (PARI eFlow® rapid, PARI GmbH, Starnberg, Germany). Briefly, the nebulizer reservoir was filled with 1 mL of a phosphate buffered saline dispersion of the peptide (1 mg/mL). The nebulizer device was connected to the induction port of the NGI and operated with a vacuum pump at a fixed flowrate of 15 L/min. The aerosol was drawn through the impactor for 5 min until dry. The peptide that remained aerosolized (i.e., inside the nebulizer reservoir, deposited on the seven stages of the NGI and in the induction port) was quantitatively recovered and quantified by HPLC/UV spectrophotometry. HPLC/UV involved a Waters Breexe System Liquid Chromatograph equipped with a Waters 717 Plus Autosampler (40 µL injection volume) and a Shimadzu UV – vis HPLC detector online with a computerized workstation. The column used was a Jupiter® C18 widepore (300 A, 5 mm x 25 cm), the mobile phase was a mixture of Water 0.1% TFA: Acetonitrile 0.1% TFA 75:25 (v/v) with a flow rate of 1 mL/min, the column temperature was 25 °C and the detection wavelength was 220 nm. Upon emission, the experimental

mass median aerodynamic diameter ($MMAD_{exp}$) and the geometric standard deviation (GSD) were calculated according to the European Pharmacopoeia, by plotting the cumulative mass of peptide retained in each collection stage (expressed as percent of total mass recovered in the impactor) *versus* the cut-off diameter of the corresponding stage. At the used flow rate (15 L/min), the cut-off diameters of the NGI stages were 14.10 µm (S1), 8.61 µm (S2), 5.39 µm (S3), 3.30 µm (S4), 2.08 µm (S5), 1.36 µm (S6), 0.98 µm (S7). The MMAD was determined from the graph as the peptide size at which the line crosses the 50% mark; the GSD was defined as:

$$\mathrm{GSD} = (\mathrm{Size\ X}/\mathrm{Size\ Y})^{1/2}$$

where size X was the size at which the line crosses the 84% mark and size Y the size at which it crosses the 16% mark.

The emitted dose (ED) was measured as the difference between the total amount initially placed in the nebulizer and the amount recovered in the stages. The fine particle fraction (FPF) was calculated by considering the amount of peptide deposited on S3-S6 ($MMAD_{exp}$ < 5.39 µm) compared to the initial amount loaded in the nebulizer chamber, while the respirable fraction (RF) was determined by the total amount recovered from the NGI. The size distribution profile and the biological function of the peptide after nebulization with the mesh nebulizer PARI eFlow® (PARI GmbH, Gräfelfing, Germany) were assessed by dynamic light scattering (DLS, Malvern Zetasizer, Worcestershire, UK) and by measuring cAMP elevation in 16HBE14o- cells (Promega cAMP-Glo™ Assay kit, Milano, IT), respectively. Fractions were collected at the beginning, middle, and end of the nebulization process to evaluate consistency. A 20 mg/mL solution of the peptide dissolved in 2 mM PBS (0.6 mM KH_2PO_4, 1.6 mM K_2HPO_4), pH 7.4 was used for these studies.

Circular dichroism

Circular dichroism (CD) spectra were acquired using a Jasco-810 Dichrograph equipped with a Peltier thermoelectric controller (Jasco Inc., Easton, US). Measurements were conducted at 25 °C using a 0.1 cm path length quartz cuvette (Hellma GmbH, Müllheim, DE). Peptides were prepared at a final concentration of 0.2 mg/mL in 10 mM PBS (10 mM phosphates, 150 mM NaCl, pH 7.4), pH 7.4. Spectra were recorded in continuous scanning mode from 260 to 180 nm. The region between 190 and 240 nm was used to estimate the secondary structural content of the peptide via the K2D2 web server[23].

Transmission electron microscopy and dynamic light scattering

Self-assembled peptide nanostructures characterized using transmission electron microscopy (TEM) analysis. TEM imaging was performed with a JEOL 3010-UHR TEM operating at an accelerating voltage of 300.00 kV (JEOL, Tokyo, Japan). Peptide samples were prepared by dissolving the compound in water at a concentration of 0.1 mg/mL and depositing them onto carbon-coated copper grids, followed by drying. Images were acquired at nominal magnifications of ×500,000 and ×800,000. For size distribution analysis, dynamic light scattering (DLS) measurements were carried out using a Malvern Zetasizer instrument (Malvern Panalytical, Worcestershire, UK). Peptides were dissolved in 10 mM PBS (10 mM phosphates, 150 mM NaCl, pH 7.4) at a final concentration of 4 mg/mL. Prior to measurement, samples were equilibrated for 60 s to allow temperature stabilization at 25 °C.

PI3Kγ MP structure prediction

The three-dimensional structure of PI3Kγ MP was predicted using the PEP-FOLD3.5 server, a de novo modeling tool for peptide structure prediction based solely on amino acid sequence[24]. Briefly, starting from the amino acid sequence, a total of 200 simulations were performed using Generator taboo-sampling 5 (ts5) algorithm, optimized for peptides longer than 10 amino acids, to explore a wide range of conformational space. The resulting structures were clustered and ranked using the TM-score followed by performing the Model Quality assessment using Apollo[25]. The five top-scoring models, selected based on the lowest sOPEP energy and highest TM-score, were further analyzed using root-mean-square deviation (RMSD) calculations.

The RMDS of each model was compared to the RMDS of residues 126–150 of the p110γ catalytic subunit of PI3Kγ, both the protein structure predicted by AlphaFold and the crystal structure (PDB ID 7mez, RCSB database)[26]. Final structural validation and visualization were performed using PyMOL.

Docking studies

Molecular docking of PI3Kγ MP to the regulatory subunit of protein kinase A (PKA-RIIα) was performed using the High Ambiguity Driven Biomolecular DOCKing (HADDOCK) platform.

The docking protocol used the NMR-derived dimeric structure of PKA-RIIα (PDB ID: 2KYG)[27] and the predicted peptide model. The process consisted of three main stages: (i) a rigid-body docking phase (it0) with random orientation of input molecules and generation of 1000 initial models; (ii) semi-flexible refinement in torsion angle space (it1) applied to the 200 top-ranked models based on HADDOCK scoring; and (iii) final refinement in Cartesian space with explicit solvent (water) and short molecular dynamics simulations at 300 K.

During the refinement, both side chains and backbone atoms at the protein-peptide interface were allowed to move.

Final docking results were clustered based on interface ligand RMSD (iL-RMSD), by fitting the conformational changes on the interface of the receptor (PKA-RIIα) and on the interface of the partner (PI3Kγ MP). Finally, the binding poses were ranked by HADDOCK score and binding affinity was further estimated using the PROtein binDIng enerGY prediction (PRODIGY) webserver[28,29]. The top predicted complex was analyzed and validated visually using PyMOL.

Statistical analysis

Data are presented as scatter plots with bars indicating the mean ± standard error of the mean (SEM). Statistical analyses were performed using Prism software (GraphPad Software Inc.). Normality of the data distribution was assessed using the Shapiro–Wilk test. Depending on the experimental design, comparisons between groups were conducted using unpaired Student's *t* test, one-way ANOVA, or two-way ANOVA. Bonferroni post hoc correction was applied to adjust for multiple comparisons. A *p*-value less than 0.05 was considered statistically significant.

Data availability

The datasets used and/or analysed during the current study available from the corresponding author on reasonable request.

Received: 29 August 2025; Accepted: 10 April 2026
Published online: 20 April 2026

References

1. Bucko, P. J. & Scott, J. D. Drugs that regulate local cell signaling: AKAP targeting as a therapeutic option. *Annu. Rev. Pharmacol. Toxicol.* **61**, 361–379. https://doi.org/10.1146/annurev-pharmtox-022420-112134 (2021).
2. Murabito, A., Cnudde, S., Hirsch, E. & Ghigo, A. Potential therapeutic applications of AKAP disrupting peptides. *Clin. Sci.* **134**, 3259. https://doi.org/10.1042/cs20201244 (2020).
3. Ghigo, A. et al. A PI3Kgamma mimetic peptide triggers CFTR gating, bronchodilation, and reduced inflammation in obstructive airway diseases. *Sci. Transl. Med.* **14**, eabl6328. https://doi.org/10.1126/scitranslmed.abl6328 (2022).
4. Della Sala, A. et al. A nonnatural peptide targeting the A-kinase anchoring function of PI3Kgamma for therapeutic cAMP modulation in pulmonary cells. *J. Biol. Chem.* **300**, 107873. https://doi.org/10.1016/j.jbc.2024.107873 (2024).
5. Celli, B. R. & Wedzicha, J. A. Update on clinical aspects of chronic obstructive pulmonary disease. *N. Engl. J. Med.* **381**, 1257–1266. https://doi.org/10.1056/NEJMra1900500 (2019).
6. d'Angelo, I. et al. Improving the efficacy of inhaled drugs in cystic fibrosis: challenges and emerging drug delivery strategies. *Adv. Drug Deliv. Rev.* **75**, 92–111. https://doi.org/10.1016/j.addr.2014.05.008 (2014).
7. Kalafatovic, D. & Giralt, E. Cell-penetrating peptides: design strategies beyond primary structure and amphipathicity. *Molecules* **22**, 1929. https://doi.org/10.3390/molecules22111929 (2017).
8. Lopes, J. L., Miles, A. J., Whitmore, L. & Wallace, B. A. Distinct circular dichroism spectroscopic signatures of polyproline II and unordered secondary structures: applications in secondary structure analyses. *Protein Sci.* **23**, 1765–1772. https://doi.org/10.1002/pro.2558 (2014).
9. Irvine, J. D. et al. MDCK (Madin-Darby canine kidney) cells: a tool for membrane permeability screening. *J. Pharm. Sci.* **88**, 28–33. https://doi.org/10.1021/js9803205 (1999).
10. Volpe, D. A. Drug-permeability and transporter assays in Caco-2 and MDCK cell lines. *Future Med. Chem.* **3**, 2063–2077. https://doi.org/10.4155/fmc.11.149 (2011).
11. Butnarasu, C., Caron, G., Pacheco, D. P., Petrini, P. & Visentin, S. Cystic fibrosis mucus model to design more efficient drug therapies. *Mol. Pharm.* **19**, 520–531. https://doi.org/10.1021/acs.molpharmaceut.1c00644 (2022).
12. Gramegna, A. et al. Neutrophil elastase in bronchiectasis. *Respir Res.* **18**, 211. https://doi.org/10.1186/s12931-017-0691-x (2017).
13. Hobbs, C. A. et al. Identification of the SPLUNC1 ENaC-inhibitory domain yields novel strategies to treat sodium hyperabsorption in cystic fibrosis airway epithelial cultures. *Am. J. Physiol. Lung Cell. Mol. Physiol.* **305**, L990–L1001. https://doi.org/10.1152/ajplung.00103.2013 (2013).
14. Craparo, E. F. et al. Sustained-release powders based on polymer particles for pulmonary delivery of beclomethasone dipropionate in the treatment of lung inflammation. *Pharmaceutics* **15**, 1248 https://doi.org/10.3390/pharmaceutics15041248 (2023).
15. Labiris, N. R. & Dolovich, M. B. Pulmonary drug delivery. Part I: physiological factors affecting therapeutic effectiveness of aerosolized medications. *Br. J. Clin. Pharmacol.* **56**, 588–599. https://doi.org/10.1046/j.1365-2125.2003.01892.x (2003).
16. Suk, J. S. et al. The penetration of fresh undiluted sputum expectorated by cystic fibrosis patients by non-adhesive polymer nanoparticles. *Biomaterials* **30**, 2591–2597. https://doi.org/10.1016/j.biomaterials.2008.12.076 (2009).
17. Yu, T. et al. Mucus-penetrating nanosuspensions for enhanced delivery of poorly soluble drugs to mucosal surfaces. *Adv. Healthc. Mater.* **5**, 2745–2750. https://doi.org/10.1002/adhm.201600599 (2016).
18. Mall, M. A. et al. Cystic fibrosis transmembrane conductance regulator in COPD: a role in respiratory epithelium and beyond. *Eur. Respir J.* **61**, 896. https://doi.org/10.1183/13993003.01307-2022 (2023).
19. Stanford, G., Morrison, L. & Brown, C. Nebuliser systems for drug delivery in cystic fibrosis. *Cochrane Database Syst. Rev.* **11**, CD007639. https://doi.org/10.1002/14651858.CD007639.pub3 (2023).
20. Oriano, M. et al. Evaluation of active neutrophil elastase in sputum of bronchiectasis and cystic fibrosis patients: a comparison among different techniques. *Pulm. Pharmacol. Ther.* **59**, 101856. https://doi.org/10.1016/j.pupt.2019.101856 (2019).
21. Sharifian, G. M. Recent experimental developments in studying passive membrane transport of drug molecules. *Mol. Pharm.* **18**, 2122–2141. https://doi.org/10.1021/acs.molpharmaceut.1c00009 (2021).
22. Yu, S. et al. A novel liquid chromatography/tandem mass spectrometry based depletion method for measuring red blood cell partitioning of pharmaceutical compounds in drug discovery. *Rapid Commun. Mass. Spectrom.* **19**, 250–254. https://doi.org/10.1002/rcm.1777 (2005).
23. Perez-Iratxeta, C. & Andrade-Navarro, M. A. K2D2: estimation of protein secondary structure from circular dichroism spectra. *BMC Struct. Biol.* **8**, 25. https://doi.org/10.1186/1472-6807-8-25 (2008).
24. Lamiable, A. et al. PEP-FOLD3: faster de novo structure prediction for linear peptides in solution and in complex. *Nucleic Acids Res.* **44**, W449–454. https://doi.org/10.1093/nar/gkw329 (2016).
25. Wang, Z., Eickholt, J. & Cheng, J. APOLLO: a quality assessment service for single and multiple protein models. *Bioinformatics* **27**, 1715–1716. https://doi.org/10.1093/bioinformatics/btr268 (2011).
26. Rathinaswamy, M. K. et al. Structure of the phosphoinositide 3-kinase (PI3K) p110gamma-p101 complex reveals molecular mechanism of GPCR activation. *Sci. Adv.* **7**, 2563. https://doi.org/10.1126/sciadv.abj4282 (2021).
27. Corpora, T. et al. Structure of the AML1-ETO NHR3-PKA(RIIalpha) complex and its contribution to AML1-ETO activity. *J. Mol. Biol.* **402**, 560–577. https://doi.org/10.1016/j.jmb.2010.08.007 (2010).
28. Vangone, A. et al. Large-scale prediction of binding affinity in protein-small ligand complexes: the PRODIGY-LIG web server. *Bioinformatics* **35**, 1585–1587. https://doi.org/10.1093/bioinformatics/bty816 (2019).
29. Xue, L. C., Rodrigues, J. P., Kastritis, P. L., Bonvin, A. M. & Vangone, A. PRODIGY: a web server for predicting the binding affinity of protein-protein complexes. *Bioinformatics* **32**, 3676–3678. https://doi.org/10.1093/bioinformatics/btw514 (2016).

Author contributions

Alessandra Ghigo and Valentina Sala conceived and designed the overall study. Angela Della Sala carried out the core of the experiments and analyzed the data. Laura Tasca performed structure prediction and docking studies. Cosmin Stefan Butnarasu measured permeability in PAMPA assays. Gabriella Costabile and Francesca Ungaro performed Next Generation Impactor studies. Marco Mergiotti, Francesco Blasi, Andrea Gramegna, Stefano Aliberti, Sonja Visentin, Emilio Hirsch provided advice on the interpretation of data. Angela Della Sala and Alessandra Ghigo wrote the manuscript with input from coauthors. All authors reviewed and approved the final manuscript.

Funding

This work was partly funded by Kither Biotech S.r.l. and partly by research grants from Cariplo Foundation (#2018 – 0498 to E.H.), Roche Foundation (Bando Roche per la Ricerca 2019 to A.G.), Compagnia di San Paolo (CSTO161109 to E.H.), Telethon Foundation (GGP20079 to A.G.), Research Grant Ministero della Salute, Italy (RC 2023/260-01 to F.B.), Fondazione IRCCS Ca' Granda Ospedale Maggiore Policlinico Milano, Regione Lombardia Cystic Fibrosis Funding 2022 (Cod. 18563 Capitolo 13.01.1 to F.B.) and PRIN 2022 (2022WHSCL3 to S.A., F.B. and E.H.).

Competing interests

Alessandra Ghigo and Emilio Hisch are cofounders and shareholders of Kither Biotech Srl. Alessandra Ghigo and Emilio Hirsch are coinventors of the patent titled "Novel pi3k gamma inhibitor peptide for treatment of respiratory system diseases" (WO2016103176A1) relative to PI3K MP (KIT2014). Valentina Sala and Laura Tasca are employees of Kither Biotech Srl. All other authors report no conflict.

Additional information

Correspondence and requests for materials should be addressed to A.G.